Galaxy source counts at 7.7 μm, 10 μm and 15 μm with the James Webb Space Telescope

Chih-Teng Ling[1], Seong Jin Kim[1], Cossas K.-W. Wu[1,2], Tomotsugu Goto[1,2], Ece Kilerci[3],
Tetsuya Hashimoto[4], Yu-Wei Lin[1,2], Po-Ya Wang[1], Simon C.-C. Ho[1], and Tiger Yu-Yang Hsiao[1]

[1]*Institute of Astronomy, National Tsing Hua University, 101, Section 2. Kuang-Fu Road, Hsinchu, 30013, Taiwan (R.O.C.)*
[2]*Department of Physics, National Tsing Hua University, 101, Section 2. Kuang-Fu Road, Hsinchu, 30013, Taiwan (R.O.C.)*
[3]*Sabancı University, Faculty of Engineering and Natural Sciences, 34956, Istanbul, Turkey*
[4]*Department of Physics, National Chung Hsing University, 145, Xingda Road, Taichung, 40227, Taiwan (R.O.C.)*

ABSTRACT

We present mid-infrared galaxy number counts based on the Early Release Observations obtained by the James Webb Space Telescope (*JWST*) at 7.7-, 10- and 15-μm (F770W, F1000W and F1500W, respectively) bands of the Mid-Infrared Instrument (MIRI). Due to the superior sensitivity of *JWST*, the 80 percent completeness limits reach 0.32, 0.79 and 2.0 μJy in F770W, F1000W and F1500W filters, respectively, i.e., ~100 times deeper than previous space infrared telescopes such as *Spitzer* or *AKARI*. The number counts reach much deeper than the broad bump around 0.05 ~ 0.5 mJy due to polycyclic aromatic hydrocarbon (PAH) emissions. An extrapolation towards fainter flux from the evolutionary models in the literature agrees amazingly well with the new data, where the extrapolated faint-end of infrared luminosity functions combined with the cosmic star-formation history to higher redshifts can reproduce the deeper number counts by *JWST*. Our understanding of the faint infrared sources has been confirmed by the observed data due to the superb sensitivity of *JWST*.

Key words: galaxies: evolution – infrared: galaxies

1 INTRODUCTION

The James Webb Space Telescope (*JWST*, Gardner et al. 2006; Kalirai 2018) is a new generation infrared (IR) telescope launched in December 2021, and has just opened up a new window to observe the faintest IR source populations that have not been observed yet. The infrared space telescopes in the pre-JWST era, namely the Infrared Astronomical satellite (*IRAS*, Neugebauer et al. 1984), *ISO* (Kessler et al. 1996), *AKARI* (Murakami et al. 2007), *Spitzer* (Werner et al. 2004), and *Herschel* (Pilbratt et al. 2010) have showed the evolution of the luminosity functions (LFs) of infrared galaxy populations in luminosity and density (e.g., Saunders et al. 1990; Rowan-Robinson et al. 1997; Elbaz et al. 2002; Caputi et al. 2007; Goto et al. 2010; Gruppioni et al. 2010, 2011). The comparison of the predictions of galaxy formation models with the observed number density of infrared galaxies is a very useful method to understand their formation and evolution history. Therefore, source counts obtained from a deep observation are crucial to understanding the evolution of these galaxies.

The mid-IR (MIR) selected galaxies have been classified roughly into three types according to the predominant emission component contributing to the MIR range of the spectral energy distribution: (i) star-forming (SF) galaxies including starbursts with various MIR (e.g., 8 μm or 12 μm) luminosities between $10^8 - 10^{11} L_\odot$, (ii) active galaxies including type 1 and type 2 active galactic nuclei (AGNs), and (iii) composites, the mixture of the emissions from the star-forming regions and AGN activity (i.e., hot dusty torus). Mid-IR number counts of galaxies have been obtained in AKARI

bands (e.g., Wada et al. 2008; Pearson et al. 2010, 2014; Takagi et al. 2012), ISO bands (e.g., Pearson 2005), Spitzer bands (e.g., Pearson 2005). Although the lower end of the mid-IR number counts, luminosity functions (LFs), and evolution models have not been fully investigated in the pre-JWST era, they have been predicted in several studies (e.g., Gruppioni et al. 2011; Cowley et al. 2018; Shen et al. 2022).

The Mid-Infrared Instrument (MIRI, Rieke et al. 2015) of *JWST* performs imaging (Bouchet et al. 2015) with 9 bands covering the 5-28 μm wavelength range. In this work, our goal is to obtain the first galaxy number counts in 7.7 μm, 10.0 μm, and 15.0 μm from the MIR data of *JWST*. We aim to characterise the evolution of the MIR LF and luminosity density (LD) up to a new sensitivity limit that is just available with *JWST*. This paper is organised as the following: In §2 we present the *JWST* data, source extraction and the completeness of our source detection. In §3, we compare the observed source counts with the model predictions from the literature and discuss our results. Our conclusion is given in §4. We follow Cowley et al. (2018) whose model we compare with, adopting the *Planck15* cosmology (Planck Collaboration et al. 2016), i.e., Λ cold dark matter cosmology with $(\Omega_m, \Omega_\Lambda, \Omega_b, h) = (0.307, 0.693, 0.0486, 0.677)$, unless otherwise mentioned.

2 DATA ANALYSIS

2.1 Source extraction

We use the publicly available *JWST* Early Release Observations (ERO) image of Stephan's quintet[1] observed in F770W, F1000W and F1500W broadband filters centred at 7.7 μm, 10.0 μm and 15.0 μm wavelengths, respectively. With *JWST* MIRI, Stephan's quintet is imaged separately in two components, Hickson Compact Group 92 and a foreground galaxy NGC 7320. The IDs of the two images are jw02732-o002_t001 and jw02732-o006_t001, respectively. Hereafter we use '002' and '006' for jw02732-o002_t001 and jw02732-o006_t001, respectively.

Since we aim to detect sources to the faintest limit observed with these filters, we perform our own source extraction as described in the following paragraph rather than using the public source catalogue. First, we mask Stephan's quintet in the centre of the images and foreground extended objects to define the field regions. The masked parts of the images are shown in Figure 1, where regions within red ellipses and outside green boxes are masked and discarded. After removing foreground objects, we have 6924 arcsec^2 and 9764 arcsec^2 sky coverage for image 002 and image 006, respectively. We utilise Source-Extractor V2.19.5 (Bertin & Arnouts 1996) to extract sources in these fields. Following the *JWST* public catalogue, we measure source fluxes from apertures that include 70% energy of the simulated *JWST* MIRI point spread function (PSF, Perrin et al. 2014) for better statistics of the source counts. Parameters that are specified in Source-Extractor are listed in Table 1. DETECT_THRESH in Table 1 stands for how many times the pixel value above the root mean square (RMS) of the background would be considered as a detected source in Source-Extractor. A value of 1.75 is applied here for every filter to detect sources that are not picked up by the official catalogue. The background RMS estimation is determined by BACK_SIZE and BACKPHOTO_THICK in Table 1. The former indicates the size of the neighbourhood of the source to be used in background calculations and the latter affects the width of the annulus of background estimation in pixel unit. The pixel scale is 0.1109 arcsec in all filters. Other unmentioned parameters remain the default value of Source-Extractor. Please refer the manual (Holwerda 2005) and the document[2] of Source-Extractor for the detail of other parameters.

Examples of extracted sources in each filter from image 002 are presented in Figures 2, 3 and 4. These objects are randomly selected by their fluxes. The fluxes of objects in the first row are about the 80% completeness limit of each filter (as described in Section 2.2), while the fluxes of objects in the second row are around ten times higher than those in the first.

2.2 Completeness

The completeness of the source detection is not provided in the public *JWST* source catalogue. Therefore, we estimate the completeness as a function of flux density based on our source extraction. The derived source count is corrected based on completeness. To estimate the completeness of our extracted source catalogue, we adopt the artificial source method described in Takagi et al. (2012). We randomly distribute 20 artificial point sources in each image, avoiding placement on the image edges or on the masks. The sources are generated
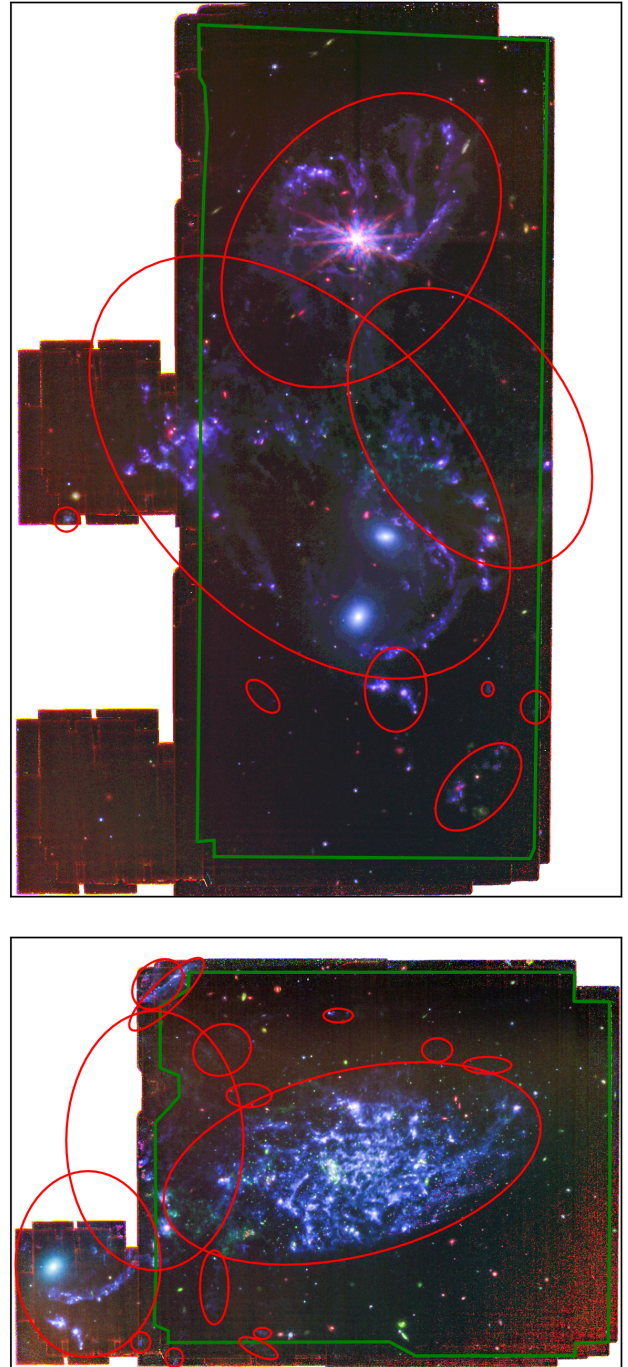
Figure 1. The mask on the false-colour images of Stephan's quintet with red (F1500W), green (F1000W) and blue (F770W). Upper: image 002; lower: image 006. Regions within red ellipses and outside green boxes are masked and not used in our analysis. The same mask is applied for all 3 filters.

from simulated *JWST* MIRI PSF, where we assume a flat spectrum. For each filter in each image, we executed the Source-Extractor in the same way as we performed the source detection and quantify the fractions of artificial sources recovered. This process is repeated 400 times with varying flux ranging from 10 nJy to 0.1 mJy in each filter and each image, with a total of 8000 artificial sources implanted.
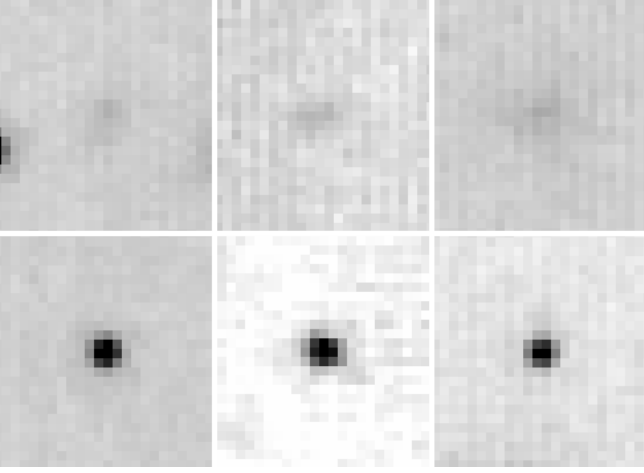
Figure 2. Examples of detected sources in field 002 at the 7.7-μm band (F770W). The fluxes of objects are ~ 0.40 μJy in the first row and ~ 4.0 μJy in the second row. All images have a field-of-view of 2×2 arcsec^2.
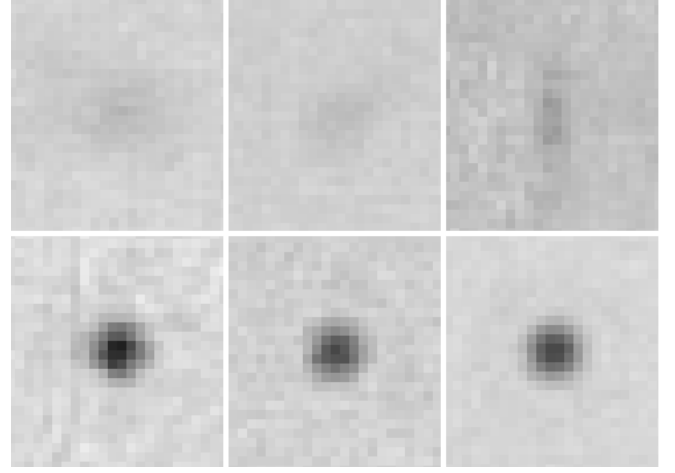
Figure 4. Examples of detected sources in field 002 at the 15-μm band (F1500W). The fluxes of objects are ~ 2.0 μJy in the first row and ~ 20 μJy in the second row. All images have a field-of-view of 2×2 arcsec^2.
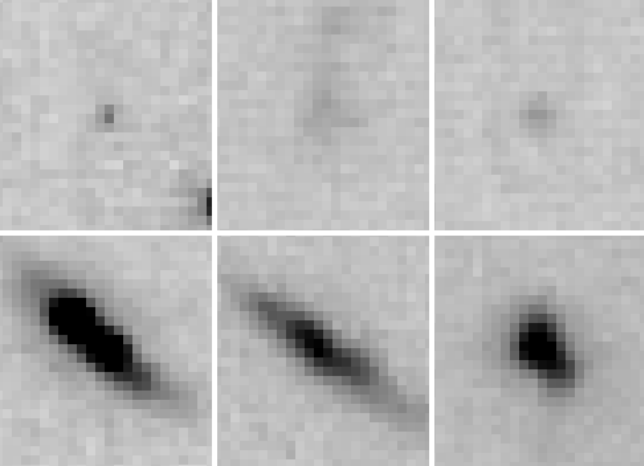
Figure 3. Examples of detected sources in field 002 at the 10-μm band (F1000W). The fluxes of objects are ~ 0.79 μJy in the first row and ~ 7.9 μJy in the second row. All images have a field-of-view of 2×2 arcsec^2.
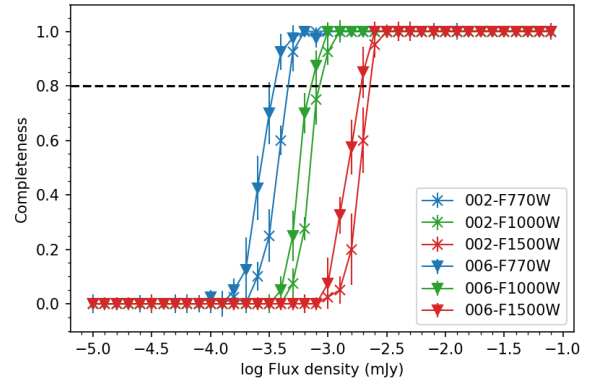
Figure 5. Source completeness of the field regions in Stephan's quintet images with a bin width of $\Delta \log(f_\nu/\text{Jy}) = 0.1$ dex. Asterisk and triangle markers indicate the images, 002 and 006, respectively. The different filters are plotted in blue (F770W), green (F1000W), and red (F1500W). The black dashed line shows our criterion of the 80% completeness.

Parameter Name	Common to the all filters		
DETECT_THRESH	1.75		
DEBLEND_NTHRESH	48		
DEBLEND_MINCONT	0.0008		
BACK_SIZE	3		
BACK_FILTERSIZE	3		
BACKPHOTO_TYPE	LOCAL		
BACKPHOTO_THICK	12		
FILTER_NAME	gauss_2.5_5×5.conv		
	F770W	F1000W	F1500W
PHOT_APERTURES [pix]	5.78	7.62	11.49

Table 1. Parameters specified in Source-Extractor.

This number is comparable to Takagi et al. (2012), considering the difference in the sky coverage.

The obtained completeness is presented in Figure 5, wherein the 006 field is slightly deeper than the 002 field in all three filters. In the 002 (006) fields, the 80 percent completeness limit reaches 0.50 (0.32), 0.79 (0.79), and 2.51 (2.00) μJy in F770W, F1000W and F1500W filters, respectively. These are slightly better than the sensitivity values in the MIRI instrument handbook[3], where the point source detection limits (SN = 10) are 0.58, 1.2, and 3.4 μJy, respectively, when scaled to the 2664 sec exposure time for each filter. In the following source count analysis described in Section 3, the number count of each flux bin is weighted by its completeness. However, we only use sources up to 80 percent of completeness limits.

---

[3] http://web.physics.ucsb.edu/~cmartin/data/4clm/MIRI._Cycle1.pdf
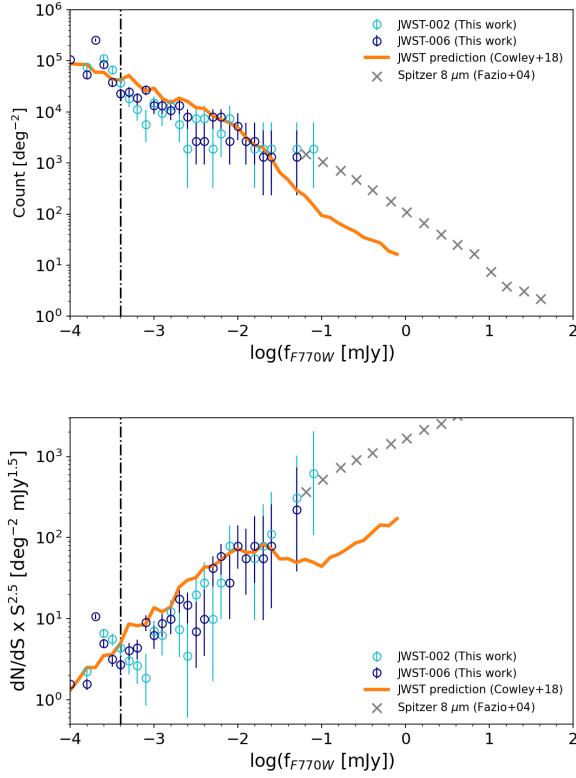
Figure 6. Source counts and models in the 7-μm band (F0700W). The top panel shows the number of sources per deg^2 in each flux bin of $\Delta \log(f_\nu/\mathrm{Jy}) = 0.1$ dex. Open circles indicate the source counts using the *JWST* data in this work. The orange line shows the prediction (differential count) from Cowley et al. (2018). We also compare with the *Spitzer* 8 μm source counts for the Boötes field ($\times$ symbol) from Fazio et al. (2004), where stars dominate the bright end. The vertical (dot-dashed) line indicates the *JWST* 80% completeness level of the source detection (002 field) derived in this work. The bottom panel shows the differential source counts normalized to the Euclidean space.

Figure 7. Same as Figure 6, but for 10-μm band (F1000W). The dark grey curve from Gruppioni et al. (2011) is consistent with the observed number counts (open circles), where we linearly extrapolate the model prediction to the low-flux end (shown as a dark grey dashed line). We also compare with the 11μm (S11 band of *AKARI*) source counts (+ symbol) from Takagi et al. (2012). The vertical (dot-dashed) line indicates the *JWST* 80% completeness level of the source detection (002 field) derived in this work.

3 RESULTS AND DISCUSSION

We present the derived number counts in light/dark blue hollow circles (002/006 fields) in Figures 6-8. The error bars of our number counts are obtained based on Gehrels (1986).

To compare with the observed source counts, we overplot source count models for MIRI's F1000W and F1500W filter bands, taken from Figures 14 and 5 of Gruppioni et al. (2011), respectively. They employed local luminosity functions (LLFs) and backward evolution for galaxies and AGNs. The 10- and 15-μm LLFs parameters are determined for five representative populations of IR galaxies, including spiral galaxies, starburst galaxies, low-luminosity AGNs, type 1 AGNs and type 2 AGNs, based on the previous *Spitzer* and *Hershel* data. The luminosity and density evolution follow their equations 2 and 3, with the model parameters presented in their Table 2. We also overplot model predictions from Cowley et al. (2018). They started from the GALFORM model (Cole et al. 2000), embedded within a dark matter only simulation (800 Mpc^3) with a halo mass resolution of $M_{\mathrm{halo}} > 2 \times 10^9$ h^{-1} M$_\odot$ provided by Baugh et al. (2019). To compute SEDs, they used the spectrophotometric radiative transfer code GRASIL (Silva et al. 1998).

Immediately noticeable in our results is the depths of *JWST*. While the brightest data points from *JWST* (this work) are around 0.1 mJy, it is already comparable to the deepest flux densities of the overplotted previous works from *Spitzer* (Fazio et al. 2004) and *AKARI* (Takagi et al. 2012). The *JWST* data continue to $\sim$ μJy levels. This has been shown in Figures 2-4, where the sources near (and ten times brighter) the *JWST* 80% completeness limit of each filter are all reliably detected in those post-stamp images. The source counts obtained in this work are well connected to the result from previous observations, (i.e., Fazio et al. 2004; Takagi et al. 2012; Elbaz et al. 1999; Gruppioni et al. 2002; Pearson et al. 2010), and extends the source counts to about two orders below than the literature.

In Figures 7 and 8, the derived number counts agree well with the model prediction for *JWST* in the dark grey line (Gruppioni et al. 2011), which were based on the infrared data from the previous generation satellites (*Spitzer*/*AKARI*; Gruppioni et al. 2010). Furthermore, our observational results also agree well with the predictions from the dark matter simulation with an embedded semi-analytical calculation (Cowley et al. 2018) in all Figures 6-8. The agreements show that our understanding of the faint population of infrared galaxies based on the previous data was correct. It is a great achievement of *JWST* to confirm models by directly detecting faint population of infrared galaxies undetectable with previous telescopes (<0.1 mJy).

We find that number counts agree well with previous empirical
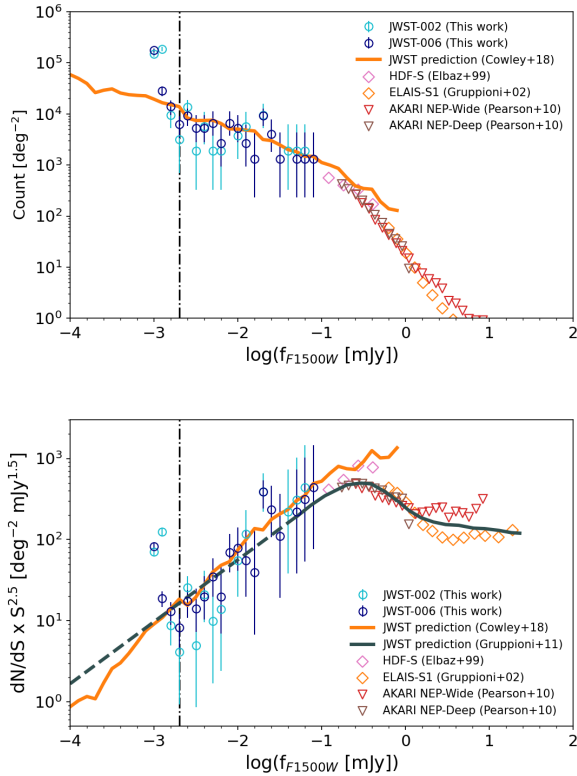
Figure 8. Same as Figure 6, but for 15-μm band (F1500W). The dark grey curve from Gruppioni et al. (2011) shows a reasonable agreement with our observed number counts (open circles), where we linearly extrapolate the model prediction to the low-flux end (shown as a dark grey dashed line). The previous source counts from Elbaz et al. (1999, pink diamonds), Gruppioni et al. (2002, orange diamonds) and Pearson et al. (2010, inverted triangles) are also compared. The vertical (dot-dashed) line indicates the *JWST* 80% completeness level of the source detection (002 field) derived in this work.

models. However, the models for the number counts are derived from a number of parameters such as luminosity evolution, density evolution, and the faint-end of LFs. These parameters degenerate in the number counts. The next important step is to disentangle these parameters by using photometric redshifts, and SED fitting techniques. The evolution of infrared LFs of different populations of infrared galaxies will be revealed in the future using the *JWST* data, once its data become available in more filters.

4 CONCLUSIONS

With the deep MIR data from the *JWST* ERO, we obtained the first source counts at 7.7 μm, 10.0 μm and 15.0 μm to characterise the source counts to the low flux limit of 0.4 μJy that has been unreachable with previous satellites. We measure 80% completeness limits to be 0.40, 0.79, and 2.0 μJy in F770W, F1000W and F1500W filters, respectively. Our results agree well with models based on previous infrared satellite data (e.g., *Spitzer* and *AKARI*), confirming our understanding of the faint infrared population of galaxies.

DATA AVAILABILITY

Early Release Observations obtained by *JWST* MIRI are publicly available at https://www.stsci.edu/jwst/science-execution/approved-programs/webb-first-image-observations. Other data underlying this article will be shared upon reasonable request to the corresponding author.

REFERENCES

Baugh C. M., et al., 2019, MNRAS, 483, 4922
Bertin E., Arnouts S., 1996, A&AS, 117, 393
Bouchet P., et al., 2015, PASP, 127, 612
Caputi K. I., et al., 2007, ApJ, 660, 97
Cole S., Lacey C. G., Baugh C. M., Frenk C. S., 2000, MNRAS, 319, 168
Cowley W. I., Baugh C. M., Cole S., Frenk C. S., Lacey C. G., 2018, MNRAS, 474, 2352
Elbaz D., et al., 1999, Astron. Astrophys., 351, L37
Elbaz D., Cesarsky C. J., Chanial P., Aussel H., Franceschini A., Fadda D., Chary R. R., 2002, A&A, 384, 848
Fazio G. G., et al., 2004, ApJS, 154, 39
Gardner J. P., et al., 2006, Space Sci. Rev., 123, 485
Gehrels N., 1986, ApJ, 303, 336
Goto T., et al., 2010, A&A, 514, A6
Gruppioni C., Lari C., Pozzi F., Zamorani G., Franceschini A., Oliver S., Rowan-Robinson M., Serjeant S., 2002, MNRAS, 335, 831
Gruppioni C., et al., 2010, A&A, 518, L27
Gruppioni C., Pozzi F., Zamorani G., Vignali C., 2011, MNRAS, 416, 70
Holwerda B. W., 2005, Source Extractor for Dummies v5, doi:10.48550/ARXIV.ASTRO-PH/0512139, https://arxiv.org/abs/astro-ph/0512139
Kalirai J., 2018, Contemporary Physics, 59, 251
Kessler M. F., et al., 1996, A&A, 315, L27
Murakami H., et al., 2007, PASJ, 59, S369
Neugebauer G., et al., 1984, ApJ, 278, L1
Pearson C., 2005, MNRAS, 358, 1417
Pearson C. P., et al., 2010, A&A, 514, A8
Pearson C. P., et al., 2014, MNRAS, 444, 846
Perrin M. D., Sivaramakrishnan A., Lajoie C.-P., Elliott E., Pueyo L., Ravindranath S., Albert L., 2014, in Oschmann Jacobus M. J., Clampin M., Fazio G. G., MacEwen H. A., eds, Society of Photo-Optical Instrumentation Engineers (SPIE) Conference Series Vol. 9143, Space Telescopes and Instrumentation 2014: Optical, Infrared, and Millimeter Wave. p. 91433X, doi:10.1117/12.2056689

Pilbratt G. L., et al., 2010, A&A, 518, L1

Planck Collaboration et al., 2016, A&A, 594, A13

Rieke G. H., et al., 2015, PASP, 127, 584

Rowan-Robinson M., et al., 1997, MNRAS, 289, 490

Saunders W., Rowan-Robinson M., Lawrence A., Efstathiou G., Kaiser N., Ellis R. S., Frenk C. S., 1990, MNRAS, 242, 318

Shen X., et al., 2022, MNRAS, 510, 5560

Silva L., Granato G. L., Bressan A., Danese L., 1998, ApJ, 509, 103

Takagi T., et al., 2012, A&A, 537, A24

Wada T., et al., 2008, PASJ, 60, S517

Werner M. W., et al., 2004, ApJS, 154, 1

This paper has been typeset from a TEX/LATEX file prepared by the author.